Journal of Energy Storage 21 (2019) 510–518

Contents lists available at ScienceDirect

Journal of Energy Storage

journal homepage: www.elsevier.com/locate/est

Remaining useful life prediction for lithium-ion batteries based on a hybrid model combining the long short-term memory and Elman neural networks

Xiaoyu Li[a,b], Lei Zhang[a,b,*], Zhenpo Wang[a,b,*], Peng Dong[a,b]

[a] National Engineering Laboratory for Electric Vehicles, School of Mechanical Engineering, Beijing Institute of Technology, Beijing, 100081, China
[b] Collaborative Innovation Center of Electric Vehicles in Beijing, Beijing Institute of Technology, Beijing, 100081, China

ARTICLE INFO

Keywords:
Electric vehicles
Lithium-ion batteries
Elman neural network
Long short-term memory
Remaining useful life

ABSTRACT

This paper presents a novel hybrid Elman-LSTM method for battery remaining useful life prediction by combining the empirical model decomposition algorithm and long short-term memory and Elman neural networks. The empirical model decomposition algorithm is employed to decompose the recorded battery capacity verse cycle number data into several sub-layers. The recurrent long short-term memory and Elman neural networks are then established to predict high- and low-frequency sub-layers, respectively. Comprehensive battery test datasets have been collected and used for model parameterization and performance evaluation. The comparison results indicate that the proposed hybrid Elman-LSTM model yields superior performance relative to the other counterparts and can predict the battery remaining useful life with high accuracy. The relative prediction errors are 3.3% and 3.21% based on two unseen datasets, respectively.

1. Introduction

Lithium-ion batteries are being extensively used as power sources in electric vehicles (EVs), thanks to their advantages of high energy and power density, low self-discharge rate and no memory effect relative to other battery chemistries [1–4]. Nevertheless, they endure continuous performance degradation in terms of capacity fade and/or internal resistance increase throughout their service life due to the ever-presence of side reactions. These would correspondingly curtail the driving range per charge and power capability of EVs that represent two major concerns preventing their mass-adoption. Normally, a capacity fade of 20% and/or an internal resistance increase of 100% would indicate the End-of-Life (EoL) for lithium-ion batteries in EV application [5–7]. Conventionally, aged batteries are more prone to fault occurrence and even severe safety issues. Hence, battery diagnosis (State-of-Health monitoring, SOH monitoring) and prognostics (Remaining useful life prediction, RUL prediction) are imperative to determining the time for maintenance and replacement of battery systems [8–10]. Particularly, the latter indicates the service life available, always in terms of cycles, before the battery reaches its EoL, and bears significance for ensuring safe and reliable operation of battery systems in EVs.

A battery aging model capable of capturing degradation characteristics of lithium-ion batteries needs to be established in order to predict battery RUL. The aging model can be built as an auto-regressive system that can predict the degradation characteristics of batteries based on measurement data as inputs [11,12]. It is well acknowledged that the actual battery capacity is strongly coupled with the number of charging/discharging cycles, in addition to other operating conditions such as charge/discharge rates and temperature, etc. Thus, the battery RUL can be predicted through recorded data describing the relationship between the actual capacity and the underlying cycle number [13]. However, the recoded data is often non-stationary and corrupted with noises and outliers such that it poses a great challenge to determine a reliable trajectory for RUL prediction. Besides, another challenge lies in how to store and update the effective features based on the recorded data through learning of long-term correlation. Therefore, it is meaningful to predict the nonlinear RUL trend by extracting features from the recorded data. It is worth noting that the battery RUL prediction can be performed on either capacity fade or internal resistance increase. At this stage, battery capacity is more concerned than internal resistance since the former largely defines the mileage per charge for EVs or service time per charge for portable electronics while the latter is closely related to the available power. It would be more meaningful to predict the battery RUL on the criterion of capacity fade, which is adopted in this study. Typically, RUL prediction methods can be classified into two main categories: model-based and data-driven methods.

The model-based methods usually combine mathematical models with advanced filtering techniques such as particle filter algorithms to

* Corresponding authors at: National Engineering Laboratory for Electric Vehicles, 5 Zhongguancun South St., Haidian District, Beijing, 100081, China.
E-mail addresses: lei_zhang@bit.edu.cn (L. Zhang), wangzhenpo@bit.edu.cn (Z. Wang).

https://doi.org/10.1016/j.est.2018.12.011
Received 23 July 2018; Received in revised form 27 November 2018; Accepted 11 December 2018
Available online 31 December 2018
2352-152X/

track the battery degradation trend. For example, Enrico et al. [14] used the particle filter and the Monte Carlo algorithm in combination to predict the battery RUL in the Bayesian framework. The Monte Carlo algorithm was used to emulate battery dynamics while the particle filter was leveraged to estimate the posterior probability density and predict the time evolution of battery degradation. Analogously, Selina et al. [15] proposed a naive Bayesian (NB) method for battery RUL prediction under the constant discharging condition. For the sake of improving the accuracy of battery RUL prediction, the unscented particle filter (UPF) was introduced to obtain the battery RUL based on a general degradation model [16]. Owing to the limited knowledge of the underlying mechanisms of battery degradation, the employed mathematical model cannot accurately reflect the characteristics of parameters evolution with the decreased capacity. To solve this issue, the Bayesian information criterion (BIC) was employed to balance the model accuracy and complexity [17]. Similarly, Lyu et al. [18] proposed an electrochemical model to simulate the battery charging/discharging process, based on which a novel particle filter framework was proposed to estimate the model parameters that are indicative of battery degradation. Also based on an empirical capacity degradation model, Zhang et al. [19] presented an improved unscented particle filter (IUPF) algorithm with the Markov Chain Monte Carlo (MCMC) for battery RUL estimation. The MCMC was employed to solve the particle impoverishment for the IUPF algorithm that was capable of battery RUL prediction. Hu et al. [20] proposed a Gauss-Hermite particle filter method to forecast the battery capacity fade for battery RUL prediction. Despite that the model-based RUL prediction has made substantial progress, there still exist two main drawbacks that hinder their feasibility in practical applications. That is, the commonly-used particle filter methods always suffer from the issue of particle impoverishment which easily leads to inaccurate RUL prediction [21]. Additionally, there is no accurate and universal battery degradation model that is able to describe the key parameters associated with battery aging for precise RUL prediction.

In contrast, the data-driven methods can effectively evade the above mentioned problems inherent with model-based RUL prediction approaches, which mainly rely on the data collection of measureable parameters (e.g., voltage, current, capacity, etc.) of batteries. The support vector machine (SVM) is among the most popular methods for constructing battery degradation models, which employs support vectors to map the recorded parameters with the predicted battery RUL. In this regard, Liu et al. [22] proposed an effective and flexible online training method for the relevance vector machine (RVM) algorithm to enhance the accuracy of battery RUL prediction. Recently, Liu et al. [23] extracted ten different features from aged batteries and fused those features into building a capacity degradation model based on the RVM algorithm for the sake of achieving a higher adaptability to complex operating conditions. Patil et al. [24] utilized the recorded voltage and temperature data as feature parameters, and devised an on-line multi-stage SVM method to accomplish accurate battery RUL prediction. Similarly, Dong et al. [25] presented a support vector regression-particle filter (SVR-PF) to predict the battery RUL based on the health monitoring results from a constructed capacity degradation model. Song et al. [26] introduced a hybrid method of Autoregressive model (AR) and PF algorithm to predict the long-term nonlinear degradation. Qin et al. [27] further proposed an integrated method to improve the accuracy of the SVR for battery health prediction, where the particle swarm optimization (PSO) method was employed to calculate the underlying kernel parameters. By examining these presented studies, it can be found that it is common to integrate a certain optimization method with kernel techniques in the SVM algorithms with the aim to improve the efficiency of battery RUL prediction. However, these algorithms invariably require a large quantity of recorded data to predict the battery degradation trend, and are always short of accurate battery RUL prediction within narrow windows, during which the battery RUL may endure a moderate rally from the descending trend along with the increased cycles.

To overcome the issues associated with the kernel techniques, neural network (NN) algorithms have attracted attention to predict the battery RUL. For instance, Zhao et al. [28] used a deep belief network (DBN) and a RVM to predict the battery RUL, in which the DBN was responsible for obtaining the degradation features and the RVM was used to build the battery degradation model. Liu et al. [29] used an adaptive recurrent neural network (ARNN) for battery RUL prediction by estimating the dynamic states of batteries. Generally, recurrent neural networks exhibit better accuracy than other algorithms such as RVMs and PFs due to its intrinsic property of using internal states for feature information description [30]. However, they also suffer from the loss of preceding battery degradation trend since it can merely hold the information state in a narrow window, which significantly compromises the prediction accuracy. Recently, Zhang et al. [31] proposed a novel long short-term memory (LSTM) recurrent neural network (RNN) to learn the long-term inclination of the battery degradation trend. By decomposing the battery capacity degradation data into high- and low-frequency parts, the LSTM-RNN can learn the long-term dependency on the low-frequency part while neglecting the high-frequency features.

In this study, a novel battery RUL prediction model is proposed based on the empirical mode decomposition (EMD) and the LSTM-RNN and Elman neural networks. The entire battery RUL prediction process can be divided into three steps. Firstly, the EMD algorithm is exploited to decompose the measured battery capacity verse cycle data into several intrinsic mode functions (IMFs) and a corresponding residual value, where the IMFs and the residual value can express the high- and low-frequency parts of the battery capacity series. Then, the LTSM-RNN and Elman neural networks are both employed to build sub-models based on the obtained low- and high-frequency battery capacity series, respectively. Finally, the battery RUL can be predicted by combining the results from these two sub-models.

The main contributions to the related literature can be summarized as follows: (1) A novel battery RUL predict framework is developed by combing the long short-term memory and Elman neural networks. (2) The EMD algorithm is used to decompose the non-stationary signals in time series into high- and low-frequency parts. (3) With the residual as the low-frequency information, the LSTM-RNN is applied to capturing the evolution trend of these long-term signals based on the recurrent links. (4) Since the high-frequency signals are indicative of the battery degradation characteristics along with increased cycles, the Elman neural network is used to represent the dynamics of these short-term signal fluctuations, thus improving the RUL prediction accuracy in both long and short windows.

The remainder of this paper is constructed as follows: Section II presents the battery test bench for capacity degradation data collection. Section III describes the proposed hybrid Elman-LSTM model for battery RUL prediction. Section IV elaborates the experimental verification, followed by the key conclusions summarized in Section V.

2. Battery test bench and capacity degradation data

In order to investigate the degradation characteristics of lithium-ion batteries, eight prismatic battery cells with a rated capacity of 1.1 Ah were evenly appropriated into two groups and used for battery aging tests under a well-established test protocol, and the experimental data were collected from the Center for Advanced Life Cycle Engineering (CALCE) at the University of Maryland [16]. The test protocol was composed by repeated cycling that consisted of a standard charging and discharging regime and the rest time in between. The cutoff voltages for discharge and charge were set 2.7 V and 4.2 V, respectively. The detailed specifications of the tested battery cells are summarized in Table 1.

The constant-current-constant-voltage (CC-CV) charging protocol was adopted for battery charging, which charges the battery with a

Table 1
The Specifications of the Tested Battery Cells.

Battery parameters	Value (Unit)
Rated Capacity	1100 mAh
Cell Chemistry	$LiCoO_2$ Cathode and Graphite Anode
Weight (with safety circuit removed)	21.1 g
Dimensions	5.4 mm × 33.6 mm × 50.6 mm

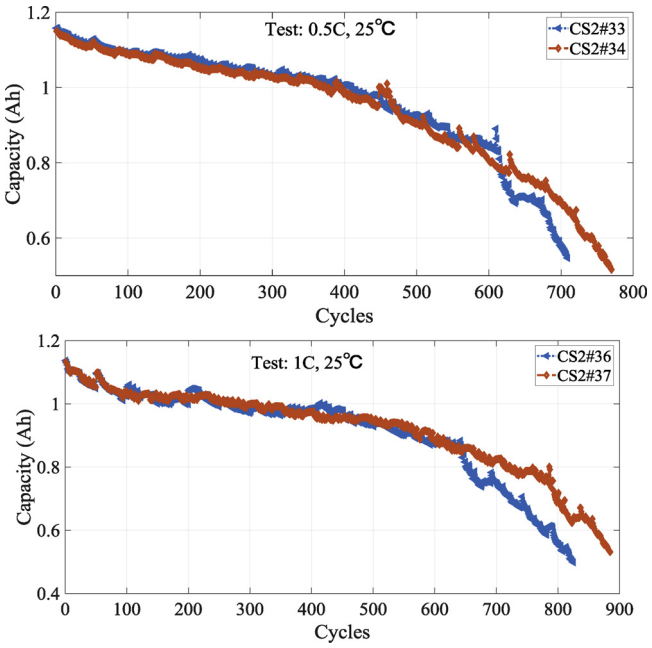

Fig. 1. Capacity degradation routes along with increased cycles under the discharging rates of 0.5C and 1C.

constant current of 0.55 A until the cutoff voltage of 4.2 V and then clips the voltage until the charging current diminishes below 0.05 A. The tested battery cells were discharged at 1C and 0.5C at a constant ambient temperature of 25℃, respectively. It is worth noting that a 1-C discharge current in Amps equates to the rated capacity of the tested battery in Ah. The actual discharged capacity of each cycle was used to indicate their degradation state verse increased cycles. The evolutions of battery capacity degradation under different discharging rates are depicted in Fig. 1. It is worth noting that the batteries CS2#33 and CS2#34 were discharged at 0.5C while the batteries CS2#36 and CS2#37 were loaded at 1C. The data collected from CS2#33 and CS2#36 were used to predict the battery RUL in real-time, whereas CS2#34 and CS2#37 were employed for model validation. As seen from Fig. 1, the tested battery cells under the same discharging rate have a very similar capacity degradation route. The battery consistency is much better at the cycles before the battery EoL as shown in each subplot while there exist obvious deviations at the cycles after the EoL. The deviations between the curves can be ascribed to the battery degradation that involves unpredictable and varied side reactions and/or structural damage, which is variable depending on specific cells. The battery inconsistency within a battery system may cause severe system-level performance degradation and safety concerns. This clearly manifests the significance of battery RUL prediction.

3. Description of the hybrid Elman-LSTM model

3.1. The hybrid Elman-LSTM model for battery RUL prediction

The major procedures for battery RUL prediction based on the proposed hybrid Elman-LSTM model is depicted in Fig. 2. More technical details will be elaborated in the following part.

(1) The EMD algorithm is applied to decomposing the measured battery capacities at different cycles into various high-frequency sub-layers (IMFs) and a low-frequency sub-layer (residual value). Those decomposition signals are regarded as independent features of the Elman-LSTM model.

(2) The high-frequency sub-layers are predicted by the Elman neural network, whilst the low-frequency sub-layer is represented by the LSTM neural network.

(3) In order to examine and confirm the performance of the proposed hybrid Elman-LSTM model, the LSTM and EMD-LSTM models are also presented for comparison purpose in this study. The LSTM neutral network estimates the battery RUL based on the original battery capacity data while the EMD-LSTM and the proposed hybrid Elman-LSTM models entail data reconstruction for battery RUL prediction.

3.2. Empirical mode decomposition

The EMD algorithm is a data-driven signal processing method that was first applied in the ocean wave-related research [32]. It has the ability to extract both high- and low-frequency components from non-stationary and non-linear signals. Through an iterative sifting procedure, the EMD algorithm is capable of decomposing the original signals into various intrinsic mode functions (IMFs) along with a relevant residual value. Usually, certain criteria are required in order to obtain a suitable IMF, i.e., the number of extrema and crossing zeros of functions should be the same or with a deviation less than 1; both upper and lower envelopes need to have zero means [33]. The detailed implementation of the EMD algorithm for battery capacity series reconstruction can be summarized as follows:

Step 1: Set $i = 1$, $C_1 = C(n)$, where $C(n)$ stands for the measured battery capacities at the *n-th* cycle.

Step 2: Search for the local maxima $C_{max,i}(n)$ and minima $C_{min,i}(n)$ of $C_i(n)$ to construct the upper and lower envelopes, respectively. The extrema are fitted by cubic splines and all the battery capacity samples are located within the upper and lower envelops. The mean value $m_i(n)$ of $C_{max,i}(n)$ and $C_{min,i}(n)$ is calculated by

$$m_i(n) = \frac{C_{max,i}(n) + C_{min,i}(n)}{2} \tag{1}$$

Step 3: Calculate the component $h_i^k(n)$ by

$$h_i^k(n) = C_i(n) - m_i^k(n) \tag{2}$$

If $h_i^k(n)$ meets the two criteria of IMFs, it is set as the i-th IMF component, $c_i(n)$. Similarly, the residual value $r_i(n)$ is calculated by

$$r_i(n) = C_i(n) - c_i(n) \tag{3}$$

Step 4: The residue $r_i(n)$ is treated as a new capacity series which is subject to the same processing as shown in steps 1–3 until forming a monotonic function. It is worth noting that $C_i(n) = r_{i-1}(n)$ for $i > 1$ and $C_i(n) = C(n)$ when $i = 1$.

Finally, the measured battery capacity data is decomposed into a set of IMFs and residual values. For instance, if the above procedures are repeated with N times, the measured battery capacity data can be restructured as

$$C(n) = \sum_{i=1}^{N} C_i(n) + r_N(n) \tag{4}$$

3.3. The Elman neural network

The Elman neural network is an artificial intelligence that has a typical global feed-forward local recurrent, in which a layer of "context units" is added to a standard feed-forward net [34]. In this way, the

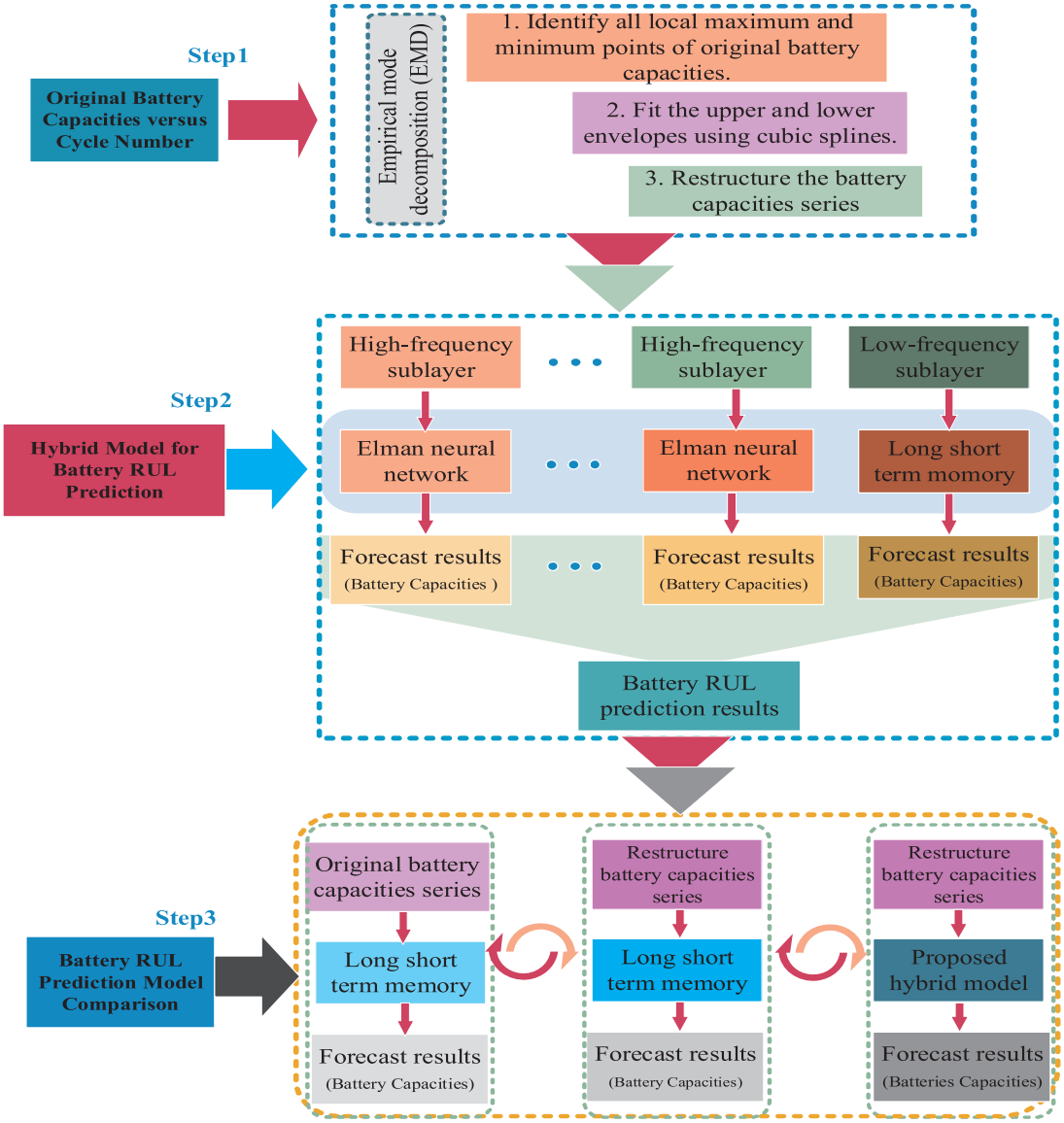

Fig. 2. Battery RUL prediction based on the proposed hybrid Elman-LSTM model.

states of the hidden units can be fed back into the hidden units during the next stage, which makes the Elman neural network own the capability of short-term memory [35]. For the battery capacity series, capacity recovery at certain cycles (See Fig. 1 for more details) can be captured by the short-term memory. Therefore, the Elman neural network becomes a good option to improve the overall accuracy of battery RUL prediction.

The structure of the standard Elman neural network is illustrated in Fig. 3. To apply the Elman neural network for battery RUL prediction, the IMFs of battery capacity series are regarded as the input features. The detailed computation process of the Elman neural network can be expressed as

$$H_n = \sigma_h(W_h x_n + U_h h_{n-1} + b_h) \tag{5}$$

$$y_n = \sigma_y(W_y h_n + b_y) \tag{6}$$

where $\boldsymbol{x}_n$ refers to the recorded battery capacity series, $\boldsymbol{h}_n$ is the hidden layer vector, $\boldsymbol{y}_n$ represents the predicted capacity series, $\boldsymbol{W}$ and $\boldsymbol{U}$ are the weigh matrices, and $\boldsymbol{b}_y$ represents the bias vector. $\boldsymbol{\sigma}$ is the logic function of the neural network, which can be calculated by

$$\sigma(x) = \frac{1}{1 + e^{-x}} \tag{7}$$

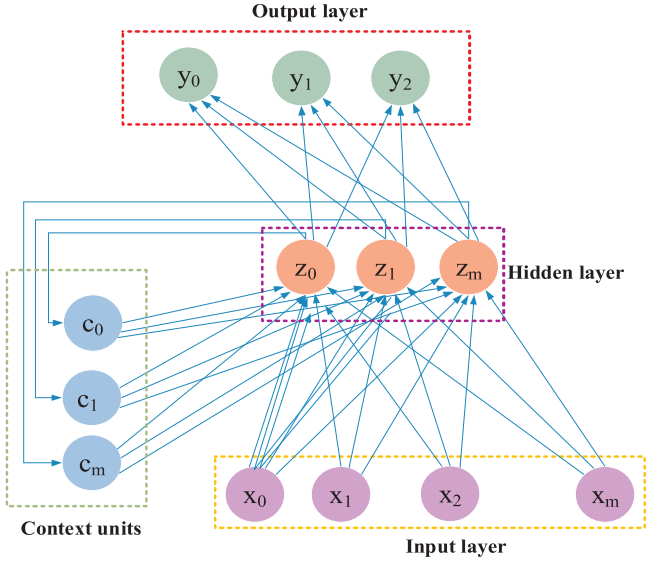

Fig. 3. Elman neural network structure.

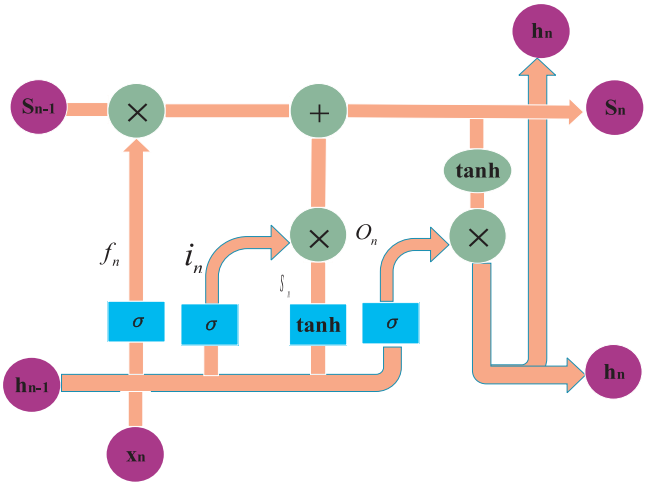

Fig. 4. The general architecture of a LSTM model.

3.4. Long short-term memory

The LSTM is a type of recurrent neural network (RNN) with good capability of solving the vanishing gradient problem [36, 37]. The general architecture of the LSTM is delineated in Fig. 4, in which the computation of S_n plays an important role. Instead of directly computing S_n from S_{n-1}, the LSTM derives S_n by adding the computed ΔS_n to S_{n-1}. Thus, S_n can be generally reckoned as an internal state, which is able to take the advantages of self-connected recurrent and fixed unit weights. Meanwhile, the internal state is capable of reserving information through the vivid structures including the input, forget and output gates. These gates are usually represented by the sigmoid functions that are activated based on the current input layer and the previous hidden layer. As a result, the LSTM can effectively learn the long-term tendency by efficiently resisting the gradient vanishing. For battery RUL prediction, the battery capacity degradation can be regarded as the time series of the LTSM.

As seen from Fig. 4, the state cells are controlled by the LSTM through the forgot and input gates. The forget gate determines how much the state of the cell at the previous moment h_{n-1} can be retained till the current moment h_n. For battery RUL prediction, the previous-moment battery capacity is controlled by the forget gate to generate the input parameters for the battery capacity prediction at the next moment. Here, the moment n is regarded as the cycle number, and the forget gate is given by

$$f_n = \sigma(W_f \cdot [h_{n-1}, x_n] + \boldsymbol{b}_f) \tag{8}$$

where $\boldsymbol{W}_f$ and $\boldsymbol{b}_f$ stand for the weight matrix and bias of the forget gate, respectively. $[h_{n-1}, x_n]$ represents the input vector, which consists in the battery capacity series along with the cycle number. The dimension of $\boldsymbol{W}_f$ is related with $[h_{n-1}, x_n]$, and it can rewritten as

$$[W_f]\begin{bmatrix} h_{n-1} \\ x_n \end{bmatrix} = [W_{fh} \quad W_{fx}]\begin{bmatrix} h_{n-1} \\ x_n \end{bmatrix} \tag{9}$$

Similarly, the input gate controls the state cells with the form of sigmoid function, which is described as

$$i_n = \sigma(W_i \cdot [h_{n-1}, x_n] + \boldsymbol{b}_i) \tag{10}$$

where $\boldsymbol{W}_i$ and $\boldsymbol{b}_i$ are the weight matrix and bias of the input gate, respectively. Then, a *tanh* layer is employed to compute the current input state cell $\widetilde{S}_n$. The current state cell S_n is calculated based on the forget and input gates and the current input cell by

$$\widetilde{S}_n = \tanh(W_c \bullet [h_{n-1}, x_n] + b_c) \tag{11}$$

$$S_n = f_n \circ S_{n-1} + i_n \circ \widetilde{S}_n \tag{12}$$

According to Eq. (12), the update state cell S_n consists of the current state cell $\widetilde{S}_n$ and long-term memory state cell S_{n-1}. The two state cells are controlled by the forget and input gates, respectively. The input gate can prevent the irrelevant information from affecting the memory process, and the long-term information can be retained through the forget gate. Meanwhile, the long-term information can affect the current output which is controlled through the output gate. The final output of the LSTM is determined by the output gate and the update state cell as

$$O_n = \sigma(W_o\,[h_{n-1}, x_n]) + b_o \tag{13}$$

$$h_n = O_n \tanh(S_n) \tag{14}$$

3.5. Prediction accuracy

After determining the structure of the Elman-LSTM model, the mean absolute percentage error (MAPE), mean absolute error (MAE) and root mean square error (RMSE) are selected to evaluate the performance of the proposed hybrid model for battery RUL prediction, which are expressed as

$$MAE = \left(\sum_{n=1}^{N} |X(n) - \hat{X}(n)|\right)/N \tag{15}$$

$$MAPE = \left(\sum_{n=1}^{N} |(X(n) - \hat{X}(n))/\hat{X}(n)|\right)/N \tag{16}$$

$$RMSE = \sqrt{\left(\sum_{n=1}^{N} |X(n) - \hat{X}(n)|^2\right)/(N-1)} \tag{17}$$

where $X(n)$ and $\hat{X}(n)$ stand for the measurement capacity series and predicted capacity series, respectively. N is the number of cycles between the first prediction cycle and the actual battery EoL. It can be noting that the accuracy of battery RUL predication can be also described by the difference between the numbers of actual and predicted cycles when the battery reaches its EoL.

4. Results and discussion

Comprehensive tests have been conducted to verify the performance of the proposed hybrid LSTM-Elman model for battery RUL prediction based on the four datasets. Firstly, the proposed hybrid model and two other LSTM models were trained and used for battery RUL prediction based on two datasets with different discharging rates. The first 360 samples of battery degradation data in each dataset were employed for model training while the remainder samples were used as testing data for model validation. In order to further examine the applicability of the proposed model to unseen datasets, the well-trained models were then applied to predicting battery RUL based on the other two datasets, respectively.

4.1. Battery RUL prediction based on the proposed hybrid Elman-LSTM model

For battery RUL prediction, the capacity degradation data of the batteries CS2#33 and CS2#36 were utilized as the training and validation sets for the LSTM, EMD-LSTM and hybrid Elman-LSTM models. All the used LSTM models including the one used in the hybrid Elman-LSTM model consist in an input layer, a hidden layer with 50 units and an output layer. The maximum iteration number and initial learning rate were all set as 80 and 0.01 for fair comparison. The Elman neural network consists of an input layer, a hidden layer with 50 units and an output layer. The first 360 cycles of battery capacities were used for model training and the predicted results by the three presented models for the following cycles until the EoL are illustrated in Figs. 5 and 6,

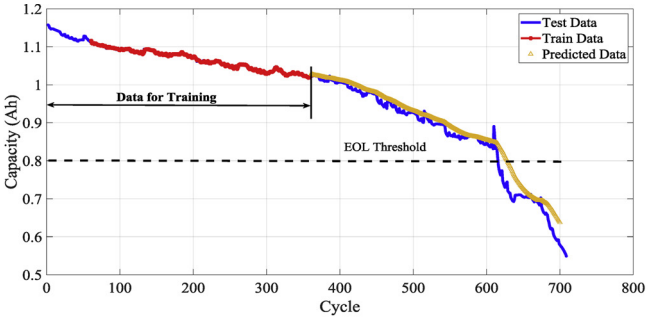

(a) The battery RUL prediction with the LSTM model.

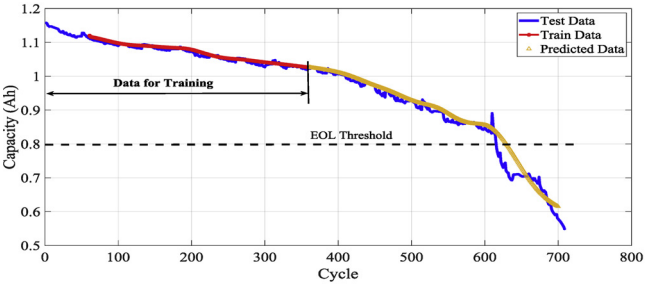

(b) The battery RUL prediction with the EMD-LSTM model.

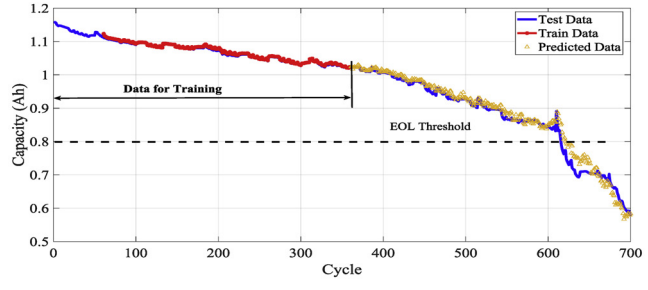

(c) The battery RUL prediction with the hybrid Elman-LSTM model.

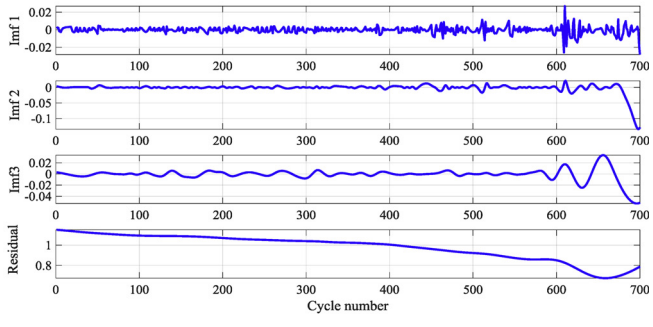

(d) Battery degradation data decomposition with the EMD algorithm.

Fig. 5. Battery RUL prediction results for the battery CS2#33 with three different models under 0.5C discharging rate. (a) The battery RUL prediction with the LSTM model. (b) The battery RUL prediction with the EMD-LSTM model. (c) The battery RUL prediction with the hybrid Elman-LSTM model. (d) Battery degradation data decomposition with the EMD algorithm.

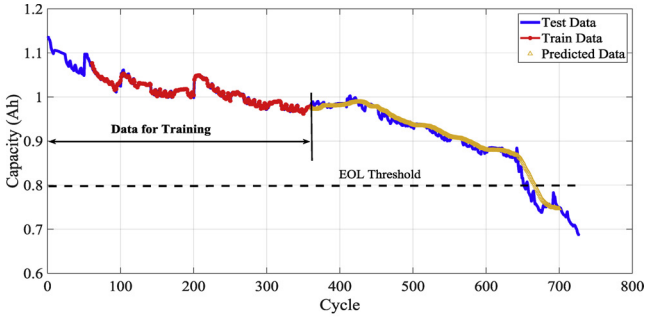

(a) The battery RUL prediction with the LSTM model.

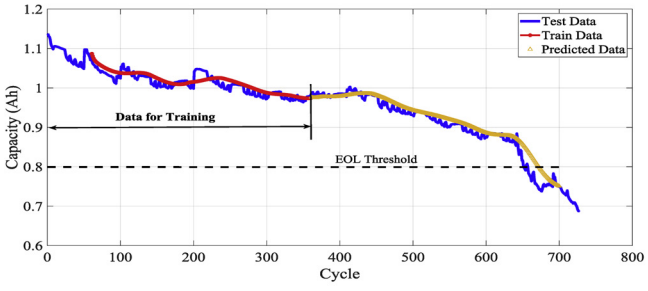

(b) The battery RUL prediction with the EMD-LSTM model

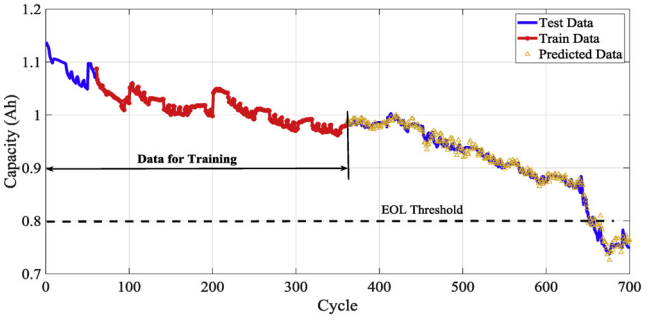

(c) The battery RUL prediction with the hybrid Elman-LSTM model.

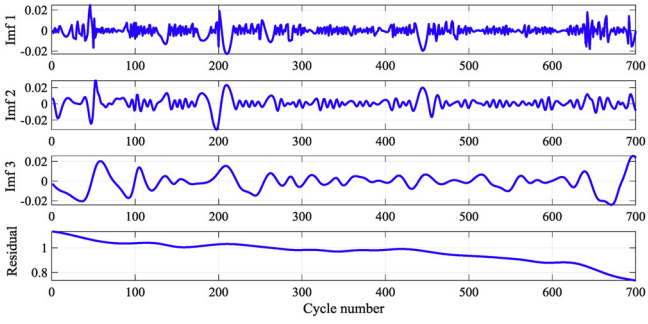

(d) Battery degradation data decomposition with the EMD algorithm.

Fig. 6. Battery RUL prediction results for the battery CS2#36 with three different models under 1C discharging rate. (a) The battery RUL prediction with the LSTM model. (b) The battery RUL prediction with the EMD-LSTM model. (c) The battery RUL prediction with the hybrid Elman-LSTM model. (d) Battery degradation data decomposition with the EMD algorithm.

respectively. It is worth noting that the presented models are all time series models, and 360 battery capacities were used as the model input to train the models that predict the battery capacities at the following cycles until EoL. The battery RUL prediction with the same number of capacities as the input can be repeatedly performed with the increasing cycle number, resulting in updated RUL prediction results.

Fig. 5 shows the battery RUL prediction results of the LSTM, EMD-LSTM and hybrid Elman-LSTM models for the battery CS2#33 with a discharging rate of 0.5C. As shown in Fig. 5(a), the battery RUL prediction based on the LSTM model starts from the 360th cycle and the prediction value drops below the EoL threshold at the 629th cycle, which has a deviation of 14 cycles (5.4%) in comparison with the actual cycle number. As seen from the results of the EMD-LSTM model in Fig. 5(b), the training data present a relatively smoother trend, and the battery is predicted to reach its EoL threshold at the 627th cycle, indicating a prediction error of 4.7%. Fig. 5(c) shows the training and

Table 2
The RUL prediction results for the battery cell CS2#33 (0.5C).

Indexes	LSTM model	EMD-LSTM model	LSTM-Elman model
MAPE (%)	2.490	3.044	1.738
MAE (Ah)	0.020	0.025	0.012
RMSE (Ah)	0.339	0.430	0.101

prediction results for battery RUL prediction based on the proposed hybrid LSTM-Elman model. After decomposing the dataset into three IMFs by the EMD algorithm, the training data of the Elman neural network is obtained, as shown in Fig. 5 (d). The predicted cycle number for reaching the battery EoL is 622, registering a deviation of 7 cycles (2.7%) in comparison with the actual test data, which evidently outperforms the other two models. This improvement can be reasonably ascribed to the capability of capturing the fluctuating trend of the measured capacity verse cycle data by the Elman neural network.

The detailed prediction performance of these models for the battery CS2#33 at 0.5C is depicted in Table 2. It can be seen that the proposed hybrid LSTM-Elman model stages the best performance for battery RUL predication in terms of MAPE, MAE and RMSE. This verifies the superiority of the hybrid LSTM-Elman model over the other counterparts.

Fig. 6 depicts the battery RUL prediction results of the LSTM, EMD-LSTM and hybrid Elman-LSTM models for the battery CS2#36 with a discharging rate of 1C, with the detailed performance listed in Table 3. The actual cycle number for reaching the battery EoL is 667. As seen from Fig. 6(a), the cycle number for reaching the battery EoL is predicted to be 675 using the LSTM model, and the corresponding MAE and RMSE are 0.011 Ah and 0.093 Ah, respectively. As shown in Fig. 6(b), the battery EoL cycle number is forecast to be 692 by the EMD-LSTM model, and the MAE and RMSE increase to 0.014 Ah and 0.202 Ah, respectively, which means a worse prediction performance than the LSTM model. This is because some meaningful samples may have been filtered out by the EMD algorithm before the model training. In contrast to the LSTM and EMD-LSTM model, the proposed hybrid Elman-LSTM model merely sees a three-cycle predication deviation with the actual test data, and the MAE and RMSE are 0.006014 Ah and 0.004014 Ah, respectively. This also validates the effectiveness of the proposed hybrid Elman-LSMT model for battery RUL prediction.

4.2. Model validity to unseen datasets

To verify the model validity of the proposed hybrid Elman-LSTM model to unseen datasets, two battery cells with the same specification have also been tested at 0.5C and 1C, respectively. The trained models from the previous parts were further utilized for battery RUL prediction based on the unseen datasets. The model inputs were updated with a window of 160 measured battery capacities to predict the battery RUL until the EoL. That is, the battery capacities beyond the cycle of 160 are all predicted values. The three different models were executed with the same manner for battery RUL prediction, with the results shown in Figs. 7 and 8. This battery RUL prediction with the same number of recorded capacities can be reiterated with the increasing cycle number, generating updated prediction results. In this study, 15 random sequences of recorded battery capacities have been used to predict the cycle number at the battery EoL. A positive RUL prediction error indicates that the predicted battery EoL is larger than the actual one while

Table 3
The RUL predication results for the battery cell CS2#36 (1C).

Indexes	LSTM model	EMD-LSTM model	LSTM-Elman model
MAPE (%)	1.279	1.615	0.680
MAE (Ah)	0.011	0.014	0.006
RMSE (Ah)	0.093	0.202	0.004

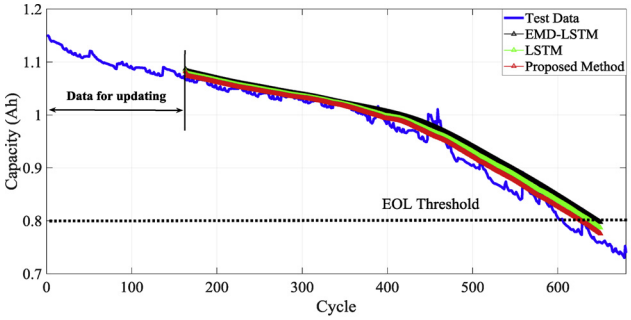

(a) The battery CS#34 RUL prediction with three battery degradation models.

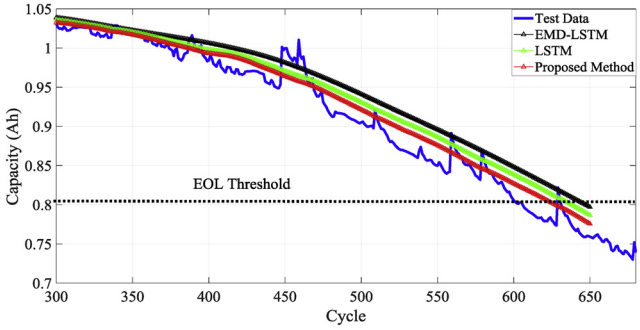

(f) Zoom-in illustration of battery RUL prediction with three battery degradation models.

Fig. 7. Battery RUL prediction results for the battery CS2#34 with three different models with a discharging rate of 0.5C. (a) The battery CS#34 RUL prediction with three battery degradation models. (b) Zoom-in illustration of battery RUL prediction with three battery degradation models.

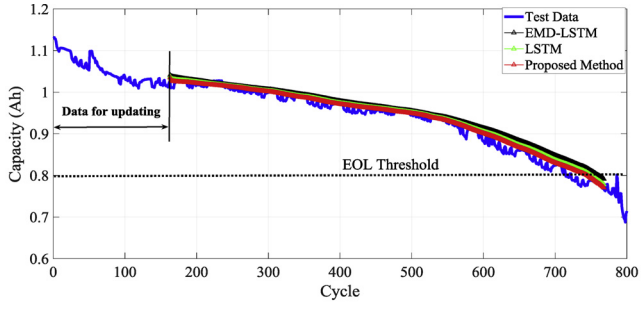

(a) The battery CS#37 RUL prediction with three battery degradation models.

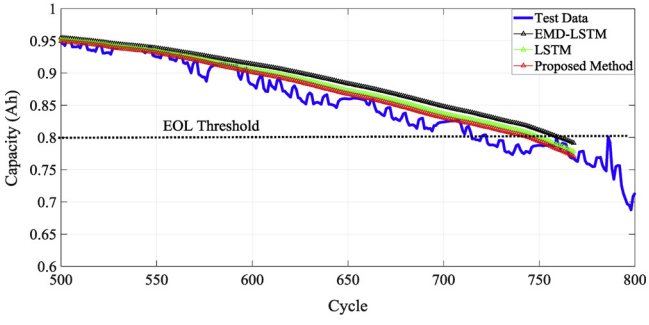

(b) Zoom-in illustration of battery RUL prediction with three battery degradation models.

Fig. 8. Battery RUL prediction results for the battery CS2#37 with three different models with a discharging rate of 1C. (a) The battery CS#37 RUL prediction with three battery degradation models. (b) Zoom-in illustration of battery RUL prediction with three battery degradation models.

Table 4
The RUL prediction results for the battery cell CS2#34 (0.5C).

Indexes	LSTM model	EMD-LSTM model	LSTM-Elman model
MAPE (%)	4.85	5.63	4.52
MAE (Ah)	0.045	0.053	0.042
RMSE (Ah)	0.988	1.163	0.915
STD (cycles)	36	30	24
95% Confidence Bound	[564 704]	[584 704]	[578 674]

Table 5
The RUL prediction results for the battery cell CS2#37 (1C).

Indexes	LSTM model	EMD-LSTM model	LSTM-Elman model
MAPE (%)	3.47	4.15	2.99
MAE (Ah)	0.033	0.037	0.030
RMSE (Ah)	1.118	1.281	0.974
STD (cycles)	23	31	18
95% Confidence Bound	[700 792]	[698 822]	[702 774]

a negative prediction error means a smaller predicted EoL than the actual one. The standard deviation (STD) is used to quantify the RUL prediction uncertainty, and a small STD means a better prediction accuracy. Besides, the 95% confidence interval (CI) is also obtained to delineate the prediction accuracy of the proposed model.

(f) Zoom-in illustration of battery RUL prediction with three battery degradation models.

The battery RUL prediction for the battery CS2#34 with the previously trained models are illustrated in Fig. 7. It is worth noting that the tested battery cells underwent 606 cycles before reaching its EoL. As seen from Fig. 7(a), the battery RUL prediction result using the LSTM model is 636 cycles, meaning a moderate prediction error. The MAE and RMSE are 0.045 Ah and 0.988 Ah, respectively. This verifies that the LSTM model has good prediction capacity for battery RUL prediction, and can be used for online implementation without a repeated training process. The projected cycle number of the EMD-LSTM model for reaching the battery EoL is 38 more cycles than the actual cycle number, indicating a bit worse performance than the LSTM model. Nevertheless, upon a close observation of Fig. 7(b), the capacity prediction exhibits a smoother trend than that under the LSTM model, which can be ascribed to the handling of the training data with the EMD algorithm. In contrast to the above mentioned models, the prediction result with the proposed hybrid Elman-LSTM model is only 20 cycles (3.3%) longer than the true value as shown in Fig. 7(a) with a 95% CI range from the 578th cycle to the 674th cycle. More detailed prediction performance of the proposed hybrid Elman-LSTM model in terms of prediction errors is listed in Table 4. It can be seen that the proposed hybrid Elman-LSTM model can outperform the other models regarding both prediction accuracy and consistency.

The battery RUL prediction for the battery CS2#37 with the previously trained models are described in Fig. 8. The battery reaches the EoL at the 715th cycle under the 1C discharging rate. As shown in Fig. 8(a), the battery EoL using the LSTM model is the 744th cycle, which is 31 cycles longer than the actual value. The MAE and RMSE for the LSTM model are 0.033 Ah and 1.118 Ah, respectively. The battery RUL prediction with the EMD-LSTM model reaches the battery EoL at the 760th cycle, which is 45 cycles longer than the actual value. The results indicate that the EMD-LSTM model exhibits poor accuracy compared with the LSTM model for battery RUL prediction. Based on the data of the battery CS2#37, the prediction result with the proposed hybrid Elman-LSTM model is only 23 cycles (3.21%) longer than the actual value. The STD is 18 cycles with a 95% CI range from the 702nd cycle to the 774th cycle. The zoom-in view shows the partial relative error remains within 0.06 Ah based on the first offline model with the battery CS2#37, as shown in Fig. 8(b). The quantitative results of the RUL prediction using the three models are listed in Table 5. It can be seen that the proposed model has excellent capability for online battery RUL prediction.

5. Conclusions

The battery RUL prediction is critical for timely maintenance and replacement of battery systems in EV application. Building an accurate and reliable prediction model holds the key for battery RUL prediction. In this paper, a hybrid RUL prediction model combining the LSTM and Elman neural networks is proposed, which can simultaneously capture the battery capacity degradation characteristics with increased cycle number in long-term and represent the capacity recovery at certain cycles in short-term. Firstly, the empirical mode decomposition (EMD) method is adopted to decompose the measured battery capacity data into various sub-layers. Then, the Elman and LSTM neural networks are employed to model the high-frequency and low-frequency sub-layers, which achieves battery RUL prediction in combination. To verify the prediction performance of the proposed hybrid Elman-LSTM model, comprehensive tests have been conducted and the LSTM and EMD-LSTM models have also been used for comparison purpose. The three models are applied to predict the battery RUL under the discharging rates of 0.5C and 1C, respectively. The results demonstrate that the proposed hybrid Elman-LSTM model can precisely realize battery RUL prediction with the deviations of 20 cycles and 23 cycles based on two unseen datasets, respectively. It is worth noting that the proposed RUL prediction method is based on the known capacities at the past cycles. These capacities can be readily available by full charging measurement or capacity estimation based on methods such as the incremental capacity analysis (ICA) and differential voltage analysis (DVA) methods. The proposed method manifests a superior performance in modeling capability and generosity to the unseen data in comparison to the other state-of-the-art models.

Acknowledgements

This study was supported in part by the National Natural Science Foundation of China under Grant U1764258.

References

[1] J.F. Peters, M. Baumann, B. Zimmermann, J. Braun, M. Weil, The environmental impact of Li-ion batteries and the role of key parameters–a review, Renew. Sustain. Energy Rev. 67 (2017) 491–506.
[2] G.E. Blomgren, The development and future of lithium ion batteries, J. Electrochem. Soc. 164 (1) (2017) A5019–A5025.
[3] J. Zhang, L. Zhang, F. Sun, Z. Wang, An overview on thermal safety issues of lithium-ion batteries for electric vehicle application, IEEE Access 6 (2018) 23848–23863.
[4] L. Zhang, X. Hu, Z. Wang, F. Sun, J. Deng, D.G. Dorrell, Multiobjective optimal sizing of hybrid energy storage system for electric vehicles, IEEE Trans. Veh. Technol. 67 (2) (2018) 1027–1035.
[5] R.R. Richardson, M.A. Osborne, D.A. Howey, Gaussian process regression for forecasting battery state of health, J. Power Sources 357 (2017) 209–219.
[6] X. Li, Z. Wang, L. Zhang, C. Zou, D.D. Dorrell, State-of-health estimation for Li-ion batteries by combing the incremental capacity analysis method with grey relational analysis, J. Power Sources 410-411 (2019) 106–114.
[7] Y. Wang, X. Zhang, C. Liu, R. Pan, Z. Chen, Multi-timescale power and energy assessment of lithium-ion battery and supercapacitor hybrid system using extended Kalman filter, J. Power Sources 389 (2018) 93–105.
[8] Y. Zhang, R. Xiong, H. He, M. Pecht, Long short-term memory recurrent neural network for remaining useful life prediction of lithium-ion batteries, IEEE Trans. Veh. Technol. (2018).
[9] S. Voronov, E. Frisk, M. Krysander, Data-driven battery lifetime prediction and confidence estimation for heavy-duty trucks, IEEE Trans. Reliab. 67 (2) (2018) 623–639.
[10] Z. Wang, J. Ma, L. Zhang, State-of-health estimation for lithium-ion batteries based on the multi-island genetic algorithm and the gaussian process regression, IEEE Access 5 (2017) 21286–21295.

[11] D. Wang, Y. Zhao, F. Yang, K.-L. Tsui, Nonlinear-drifted Brownian motion with multiple hidden states for remaining useful life prediction of rechargeable batteries, Mech. Syst. Sig. Process. 93 (2017) 531–544.
[12] R.R. Richardson, C.R. Berkl, M.A. Osborne, D. Howey, Gaussian process regression for in-situ capacity estimation of lithium-ion batteries, IEEE Trans. Ind. Informat. (2018).
[13] J. Yang, Z. Peng, H. Wang, H. Yuan, L. Wu, The remaining useful life estimation of lithium-ion battery based on improved extreme learning machine algorithm, Int. J. Electrochem. Sci. 13 (2018) 4991–5004.
[14] E. Zio, G. Peloni, Particle filtering prognostic estimation of the remaining useful life of nonlinear components, Reliab. Eng. Syst. Saf. 96 (3) (2011) 403–409.
[15] S.S.Y. Ng, Y. Xing, K.L. Tsui, A naive Bayes model for robust remaining useful life prediction of lithium-ion battery, Appl. Energy 118 (2014) 114–123.
[16] Q. Miao, L. Xie, H. Cui, W. Liang, M. Pecht, Remaining useful life prediction of lithium-ion battery with unscented particle filter technique, Microelectron. Reliab. 53 (6) (2013) 805–810.
[17] K. Chen, F. Zheng, J. Jiang, W. Zhang, Y. Jiang, K. Chen, Practical failure recognition model of lithium-ion batteries based on partial charging process, Energy 138 (2017) 1199–1208.
[18] C. Lyu, Q. Lai, T. Ge, H. Yu, L. Wang, N. Ma, A lead-acid battery's remaining useful life prediction by using electrochemical model in the particle filtering framework, Energy 120 (2017) 975–984.
[19] X. Zhang, Q. Miao, Z. Liu, Remaining useful life prediction of lithium-ion battery using an improved UPF method based on MCMC, Microelectron. Reliab. 75 (2017) 288–295.
[20] C. Hu, G. Jain, P. Tamirisa, T. Gorka, Method for estimating capacity and predicting remaining useful life of lithium-ion battery, Appl. Energy 126 (2014) 182–189.
[21] R. Khelif, B. Chebel-Morello, S. Malinowski, E. Laajili, F. Fnaiech, N. Zerhouni, Direct remaining useful life estimation based on support vector regression, IEEE Trans. Ind. Electron. 64 (3) (2017) 2276–2285.
[22] D. Liu, J. Zhou, D. Pan, Y. Peng, X. Peng, Lithium-ion battery remaining useful life estimation with an optimized relevance vector machine algorithm with incremental learning, Measurement 63 (2015) 143–151.
[23] D. Liu, Y. Song, L. Li, H. Liao, Y. Peng, On-line life cycle health assessment for lithium-ion battery in electric vehicles, J. Cleaner Prod. 199 (2018) 1050–1065.
[24] M.A. Patil, et al., A novel multistage support vector machine based approach for Li ion battery remaining useful life estimation, Appl. Energy 159 (2015) 285–297.
[25] H. Dong, X. Jin, Y. Lou, C. Wang, Lithium-ion battery state of health monitoring and remaining useful life prediction based on support vector regression-particle filter, J. Power Sources 271 (2014) 114–123.
[26] Y. Song, D. Liu, C. Yang, Y. Peng, Data-driven hybrid remaining useful life estimation approach for spacecraft lithium-ion battery, Microelectron. Reliab. 75 (2017) 142–153.
[27] T. Qin, S. Zeng, J. Guo, Robust prognostics for state of health estimation of lithium-ion batteries based on an improved PSO–SVR model, Microelectron. Reliab. 55 (9) (2015) 1280–1284.
[28] G. Zhao, G. Zhang, Y. Liu, B. Zhang, C. Hu. Lithium-ion battery remaining useful life prediction with deep belief network and relevance vector machine. *Proceedings of 2017 IEEE International Conference on Prognostics and Health Management (ICPHM 2017)*, 7–13.
[29] J. Liu, A. Saxena, G. Kai, B. Saha, W. Wang. An adaptive recurrent neural network for remaining useful life prediction of lithium-ion batteries. *Proceedings of the 2010 Annual Conference of the Prognostics and Health Management Society*.
[30] M. Rezvani, S. Lee, J. Lee, A comparative analysis of techniques for electric vehicle battery prognostics and health management (PHM), SAE Technical Paper, (2011).
[31] Y. Zhang, R. Xiong, H. He, Z. Liu, A LSTM-RNN method for the lithuim-ion battery remaining useful life prediction, 2017 Prognostics and System Health Management Conference (PHM-Harbin), (2017), pp. 1–4.
[32] N.E. Huang, et al., The empirical mode decomposition and the Hilbert spectrum for nonlinear and non-stationary time series analysis, Proc. R. Soc. Lond. A: Math. Phys. Eng. Sci. 454 (1971) (1998) 903–995.
[33] H. Liang, S.L. Bressler, R. Desimone, P. Fries, Empirical mode decomposition: a method for analyzing neural data, Neurocomputing 65 (2005) 801–807.
[34] J.L. Elman, Finding structure in time, Cogn. Sci. 14 (2) (1990) 179–211.
[35] P. Li, Y. Li, Q. Xiong, Y. Chai, Y. Zhang, Application of a hybrid quantized Elman neural network in short-term load forecasting, Int. J. Electric. Power Energy Syst. 55 (2014) 749–759.